Polish Society of Composite Materials
Polskie Towarzystwo Materiałów Kompozytowych

20: 3-4 (2020) 157-162

COMPOSITES THEORY AND PRACTICE
ISSN: 2084-6096
ISSN (online): 2299-128X

Milena Synowiec*, Karolina Zazakowny

AGH – University of Science and Technology, Faculty of Materials Science and Ceramics, al. A. Mickiewicza 30, 30-059 Kraków, Poland
**Corresponding author. E-mail: milsyn@agh.edu.pl*

Received (Otrzymano) 12.12.2020

ENHANCED VISIBLE LIGHT ABSORPTION OF SHAPE-CONTROLLED TiO_2@Fe_2O_3 COMPOSITES

This article presents titanium(IV) oxide nanocrystals in the crystalline form of anatase obtained by hydrothermal synthesis using various shape-controlling agents. Two methods were applied. In the first, diethanolamine (DEA) was used as the shape-controlling agent and titanium(IV) isopropoxide (TTIP) as the TiO_2 precursor. In the second method, carbonate ions were responsible for controlling the shape, while potassium titanate nanowires (KTNWs) were the precursor of TiO_2. The expected application of the nanocrystals was related to the absorption of visible light. Therefore, the main goal was to modify shape-controlled TiO_2 with a narrow band semiconductor providing absorption of light in that range. Based on spectrophotometric analysis, it was found that the TiO_2@Fe_2O_3 composites possess a band gap in the range between 2.21 and 2.30 eV which originates from the Fe_2O_3 nanoparticles. Moreover, a small amount of Fe^{3+} ions was incorporated into the TiO_2 lattice, as evidenced by the band gap ranging from 2.85 to 2.95 eV.

Keywords: titanium dioxide nanocrystals, narrow band gap semiconductor, hematite, visible light absorption, TiO_2@Fe_2O_3 composites

ZWIĘKSZONA ABSORPCJA ŚWIATŁA WIDZIALNEGO W KOMPOZYTACH TiO_2@Fe_2O_3 O KONTROLOWANYM KSZTAŁCIE

Przedstawiono nanokryształy dwutlenku tytanu w postaci anatazu otrzymane w wyniku syntezy hydrotermalnej przy zastosowaniu różnych środków kontroli kształtu. W pierwszej metodzie użyto dietanoloaminy (DEA) jako środka regulującego kształt i izopropanolanu tytanu(IV) (TTIP) jako prekursora TiO_2. W drugiej metodzie za kontrolę kształtu odpowiadały jony węglanowe, a prekursorem były nanodruty tytanianu potasu (KTNWs). Mając na uwadze przyszłe wykorzystanie otrzymanych nanokryształów w zastosowaniach związanych z absorpcją światła widzialnego, celem było zmodyfikowanie TiO_2 o kontrolowanym kształcie za pomocą półprzewodnika wąskopasmowego, którego absorpcja promieniowania obejmuje obszar widzialny. Uzyskane kompozyty TiO_2@Fe_2O_3 posiadają przerwę wzbronioną o wartości z przedziału od 2,21 do 2,30 eV pochodzącą od nanocząstek Fe_2O_3. Ponadto niewielka ilość jonów Fe^{3+} została wprowadzona do sieci TiO_2, o czym świadczy przerwa wzbroniona o wartości 2,85÷2,95 eV.

Słowa kluczowe: nanokryształy dwutlenku tytanu, półprzewodnik wąskopasmowy, hematyt, absorpcja promieniowania widzialnego, kompozyty TiO_2@Fe_2O_3

INTRODUCTION

Titanium dioxide is one of the most frequently used semiconductors in fields such as photocatalysis [1-3], solar cells [4], self-cleaning coatings [5], and gas sensors [6] due to its nontoxicity, chemical stability, abundance, and low cost. Many attempts have been reported to improve the properties of TiO_2 in such a manner as to meet particular requirements relevant to these applications [7, 8]. One of the methods is to control the shape of the nanocrystals and expose selected crystallographic facets characterized by different surface energies [9-13]. Nevertheless, the problem of the too wide band gap of TiO_2 (3.2 eV) corresponding only to the absorption of UV light remains unsolved. To enable the absorption of visible light, semiconductors with a narrow band gap are often used, e.g. Fe_2O_3, which is also inexpensive and environmentally friendly [14-18]. Due to its band gap equal to 2.2 eV, iron(III) oxide can absorb light of a wavelength above 560 nm [19]. TiO_2@Fe_2O_3 composites are promising materials, hence the knowledge about their interactions with light seems to be very important for future applications.

MATERIALS AND METHODS

Synthesis of TiO_2 NCs

Method 1: Diethanolamine (DEA) was used as the shape-controlling agent and titanium(IV) isopropoxide

(TTIP) as the TiO_2 precursor. Titanium(IV) oxide nanocrystals were obtained by changing two parameters: the synthesis temperature and the molar ratio of tetrabutylammonium hydroxide (TBAH) to diethanolamine TBAH:DEA. The number of TTIP moles was constant. The M1.2 sample was prepared as follows: 26.7 ml of 1.5 M TBAH and 10 ml of 10.4 M DEA were poured into a Teflon container, which was placed in an ice bath, and stirred until the solution reached 5°C. Then, 0.9 ml of TTIP was added dropwise and the reaction mixture was raised to room temperature. Next, it was transferred to a hydrothermal reactor in which the synthesis occurred at 200°C for 24 hours with a stirring speed of 500 rpm. The M2.2, M3.2, M4.2, and M5.2 samples were prepared using the same reagent concentrations, and in some cases, the reaction temperature was increased to 215°C. Only the M6.2 sample was prepared using 133.5 ml of 0.1 M TBAH, 50 ml of 0.267 M DEA, and 4.5 ml of TTIP (at 215°C for 24 h). To remove organic impurities from the surface of the freshly synthesized powders, they were washed three times with 0.1 M hydrochloric acid, distilled water, and finally with ethanol. Then, they were dried in air at 60°C for 24 hours and calcined in air at 400°C for 3 h (Table 1).

Method 2: Carbonate ions were used for shape control, while KTNWs (potassium titanate nanowires) were the precursor. To obtain the KTNWs, 160 ml of 10 M KOH and 1 g of P25 were transferred to the hydrothermal reactor in which the synthesis took place at 200°C for 16 h. Then, they were washed five times with ethanol and dried in air at 60°C for 24 hours. The S1 sample was prepared as follows: 160 ml of distilled water was poured into a Teflon container and 1.5 g of KTNWs was added. After 15 minutes of sonication, 6 g of urea was also added. Synthesis took place at 20°C for 16 h. The obtained precipitation was washed five times with ethanol and dried in air at 60°C for 24 h. Subsequent materials were obtained by increasing the amount of KTNWs (1.5 g (S1)/3.0 g (S2)/4.5 g (S3)/6.0 g (S4)), while the amount of water and urea was constant (Table 1).

Synthesis of TiO_2@Fe_2O_3 composites

TiO_2@Fe_2O_3 composites were prepared as follows: 1 g of TiO_2 powder was added to a beaker containing 50 ml of iron(III) chloride (0.0006 M) and sodium hydroxide (0.01 M) was added dropwise until the pH was 10. The precipitate was stirred for 24 h. The obtained powder was washed with distilled water until it reached the neutral pH. After that, it was dried in air at 60°C for 24 h and calcined at 350°C for 2 h (Table 1).

Characterization

The morphology of the bare and modified TiO_2 materials was investigated by means of a Nova NanoSEM 200 scanning electron microscope (SEM) equipped with a Helix detector and a field emission gun (FEG). The SEM studies were combined with energy-dispersive X-ray spectroscopy (EDX). The crystal structure of the obtained materials was investigated using an X'Pert Pro PANalytical (Philips) diffractometer equipped with a copper anode as the radiation source ($K_{\alpha 1}$ = = 0.15406 nm) in the range of 20° to 80°. Qualitative and quantitative analyses were performed using the Rietveld method, and the crystallite size was determined from the Scherer equation. The optical properties were analyzed using a Jasco V-670 UV-VIS-NIR spectrophotometer equipped with an integrating sphere (150 nm). The spectral dependence of the total reflectance $R_{tot}(\lambda)$ was measured in the range of 220÷ ÷2000 nm, and the band gap energy was calculated by differentiating total reflectance spectra $dR_{tot}/d\lambda$ and determining the positions of the maxima.

TABLE 1. **Detailed conditions of material preparation**
TABELA 1. **Szczegółowe warunki otrzymywania materiałów**

TiO_2 NC synthesis – method 1			
Sample	**TBAH:DEA molar ratio**	**Synthesis time**	**Hydrothermal synthesis temperature**
M1.2	2:5	24 h	200°C
M2.2	2:5		215°C
M3.2	10:1		200°C
M4.2	10:1		215°C
M5.2	1:10		200°C
M6.2	1:1		215°C
TiO_2 NC synthesis – method 2			
Sample	**KTNW:urea mass ratio**	**Synthesis time**	**Hydrothermal synthesis temperature**
S1	1.5:6	16 h	200°C
S2	3:6		
S3	4.5:6		
S4	6:6		
TiO_2@Fe_2O_3 composite synthesis			
Sample	**$FeCl_3$ conc. [M]**	**NaOH conc. [M]**	**Fe/Ti wt.% from EDX**
P25@Fe_2O_3	0.0006	0.01	0.012
M6.2@Fe_2O_3			0.009
S4@Fe_2O_3			0.008

RESULTS

The hydrothermal method was applied to synthesize shape-controlled TiO_2 nanocrystals. The method based on varying the ratios of bridging the ligand-to-capping agent molar ratio (TBAH-to-DEA) was used. Figure 1 shows SEM micrographs of TiO_2 nanoparticles of different shapes. The sample symbol is in the upper-left corner of the microphotograph, and the shape of the nanocrystals in the upper-right corner. When the synthesis was carried out with TBAH:DEA = 2:5 at 200°C (M1.2 sample) homogeneous spherical grains with

a size ranging from 100 to 160 nm were obtained. However, they are aggregates composed of smaller particles with a size of ca. 20÷40 nm. What is more, increasing the temperature of the processes escalates agglomeration. The M3.2 and M4.2 samples (TBAH:DEA = 10:1 at 200°C or 215°C, respectively) consist of nanorods with a length of 400÷700 nm and a width of 130÷180 nm. As can be seen in Figure 1, for the TBAH:DEA = 1:1 molar ratio, the M6.2 sample consists of nanorods with a length of 100÷240 nm and a width of 90÷100 nm. The M2.2 and M5.2 powders do not show a defined shape and are significantly agglomerated.

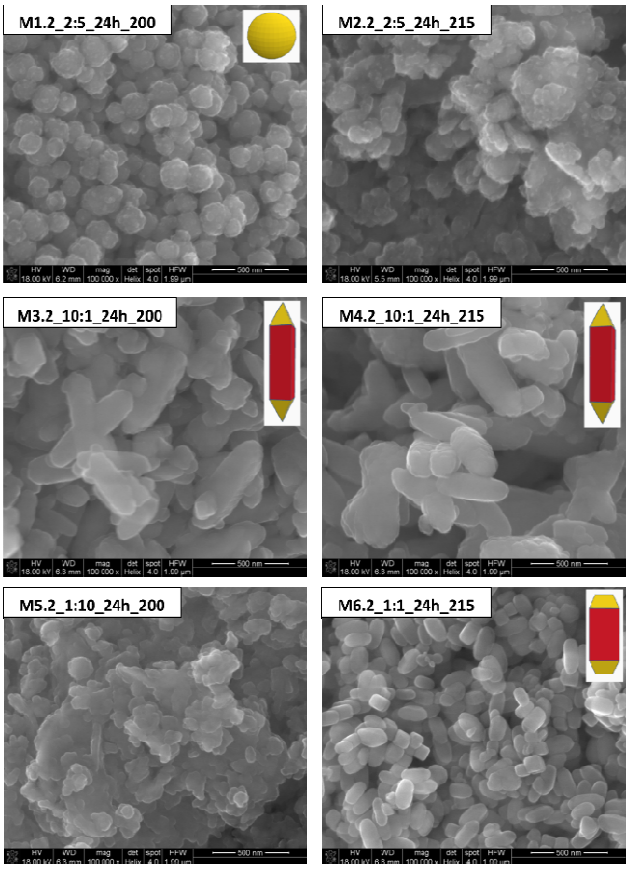

Fig. 1. SEM micrographs of TiO_2 nanocrystals synthesized from TTIP precursor. Top frame includes: sample symbol TBAH-to-DEA molar ratio synthesis time [h]_synthesis temperature [°C]

Rys. 1. Obrazy SEM nanokryształów TiO_2 zsyntetyzowanych przy użyciu prekursora TTIP. Górna ramka zawiera: symbol próbki_stosunek molowy TBAH do DEA_czas syntezy [h]_temperatura syntezy [°C]

In the second method, carbonate ions were responsible for shape control. The weight fraction of the KTNWs in relation to urea (KTNWs:urea) was varied during the synthesis of the samples. The SEM micrographs of the obtained materials are shown in Figure 2. The synthesis of the S4 sample with the largest amount of precursor (KTNWs:urea = 6:6) leads to the fabrication of titanium dioxide nanocrystals. However, the TiO_2 NCs do not exhibit a well-defined shape. There are composed of smaller particles with a size of 20÷40 nm. At a higher urea concentration (KTNWs:urea = 4.5:6, S3 sample), an undefined shape of particles was obtained as well. A further increase in the concentration of carbonate ions in the reaction solution (S2 sample) results in rod-like and spherical nanocrystals. The sample with the most homogeneous shape is S1 – the one that was synthesized using the largest amount of the shape-controlling agent (KTNWs:urea = 1.5:6). A The anatase nanocrystals, with a rod-like shape and a length of 350÷÷460 nm, are aggregates composed of smaller particles similar to all of the other discussed materials (S2-S4).

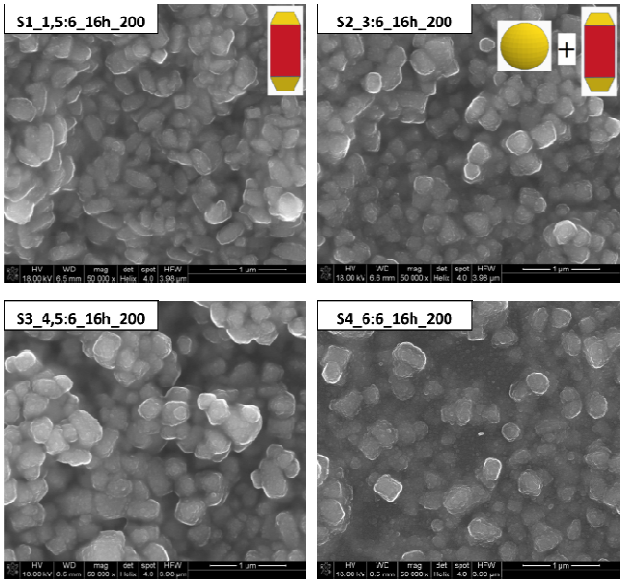

Fig. 2. SEM micrographs of TiO_2 nanocrystals synthesized from KTNW precursor. Top frame includes: sample symbol _KTNWs:urea mass ratio_synthesis time [h]_synthesis temperature [°C]

Rys. 2. Obrazy SEM nanokryształów TiO_2 zsyntetyzowanych przy użyciu prekursora KTNWs. Górna ramka zawiera: symbol próbki_ stosunek masowy KTNWs:mocznika_czas syntezy [h]_temperatura syntezy [°C]

Selected TiO_2 nanocrystals (S4, M6.2, and the commercial P25 powder) were used to be covered with Fe_2O_3 particles via the co-precipitation method. The chemical composition of the obtained TiO_2@Fe_2O_3 composites was investigated by EDX analysis. The presence of small amounts of iron(III) oxide was confirmed for all the materials. The content of Fe defined as the Fe/Ti weight percentage (wt.%) was 0.008, 0.009, and 0.012 for S4@Fe_2O_3, M6.2@Fe_2O_3, and P25@Fe_2O_3, respectively. The SEM examination did not allow to determine the distribution of the iron(III) oxide particles on the titanium(IV) oxide surface because the amount of Fe_2O_3 was too small to be detected (Fig. 3).

The XRD results for the pure TiO_2 powders are presented in Figure 4. The top and bottom bars represent the rutile (R), anatase (A) (Fig. 4a), and hematite (H) (Fig. 4b) peak positions. The qualitative analysis allowed the crystal structure of the samples to be determined. The M6.2 nanocrystals crystalize in the anatase structure, while the S4 NCs are composed of anatase, which is a major phase, and a small amount of rutile (0.3%) (Fig. 4a). The commercial P25 powder is a mixture of anatase and rutile polymorphs. The amount of Fe_2O_3 in the TiO_2@Fe_2O_3 composites was below the

detection level of the XRD method, and thus, no hematite peaks were observed. Therefore, to confirm the structure of iron(III) oxide, pure Fe_2O_3 was synthesized using the same method. The peak positions in the diffractogram (Fig. 4b) indicate single-phase α-Fe_2O_3. The sizes of the anatase and hematite crystallites were determined using the Scherrer equation. The larger crystallites, ca. 118 nm, were obtained by the second method, where the amount of KTNWs was increased.

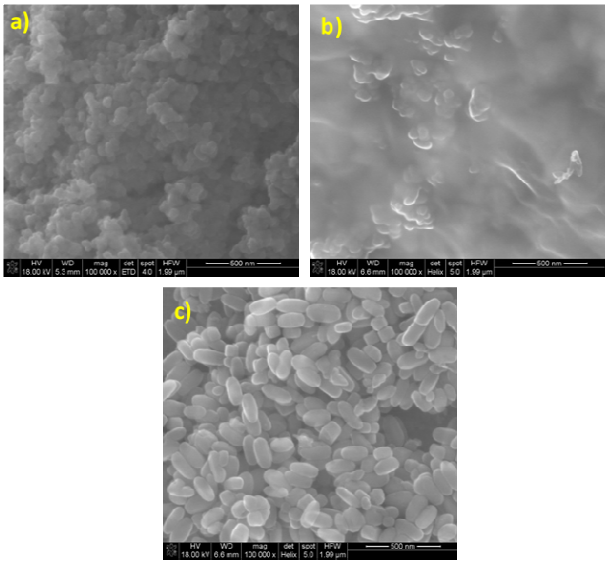

Fig. 3. SEM micrographs of Fe_2O_3-modified TiO_2 nanocrystals: a) P25@Fe_2O_3, b) S4@Fe_2O_3, c) M6.2@Fe_2O_3

Rys. 3. Obrazy SEM nanokryształów TiO_2 modyfikowanych Fe_2O_3: a) P25@Fe_2O_3, b) S4@Fe_2O_3, c) M6.2@Fe_2O_3

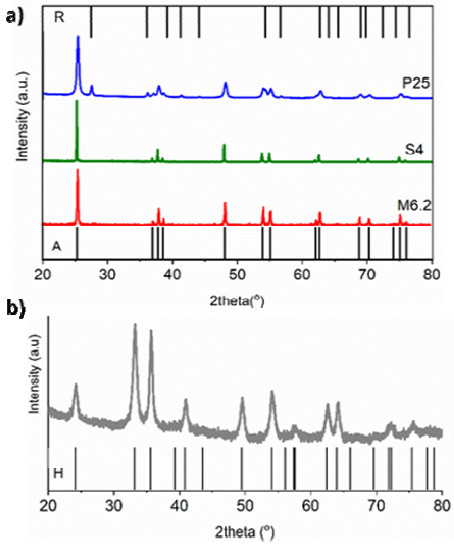

Fig. 4. X-ray diffraction patterns of: a) TiO_2 nanocrystals and P25, b) Fe_2O_3 obtained by same method as TiO_2@Fe_2O_3 composite but without addition of TiO_2 powders

Rys. 4. Dyfraktogramy: a) nanokryształów TiO_2 oraz P25, b) Fe_2O_3 otrzymanego tą samą metodą co kompozyty TiO_2@Fe_2O_3, ale bez dodatku proszku TiO_2

On the other hand, when the TBAH:DEA molar ratio was changed, the first method gave a crystal with a size of about 38 nm. It was also found that iron(III) oxide crystallites with a size of ca. 8 nm are the smallest (Table 2).

TABLE 2. **Phase composition and crystallite size calculated from Rietveld refinement for TiO_2 and Fe_2O_3 powders**

TABELA 2. **Skład fazowy oraz rozmiar krystalitów wyliczony z dopasowania Rietvelda dla proszków TiO_2 oraz Fe_2O_3**

Sample	Anatase [wt.%]	Rutile [wt.%]	Crystallite size [nm]
P25	82.1%	17.9%	12.5*/14.1**
M6.2	100%	-	37.6
S4	99.7%	0.3%	118.3
Fe_2O_3	100% hematite		8.2

*anatase, **rutile

The deposition of iron(III) oxide on the titanium(IV) oxide surface aimed to extend the absorption range from UV to visible light. However, because the light must reach both components of the composite, it is undesirable to completely cover the surface of TiO_2 by Fe_2O_3. Therefore, only a small amount of Fe_2O_3 was applied.

The spectral dependences of the total reflectance measured for the pure TiO_2 NCs and the TiO_2 NCs covered with Fe_2O_3 are presented in Figure 5a and b, respectively.

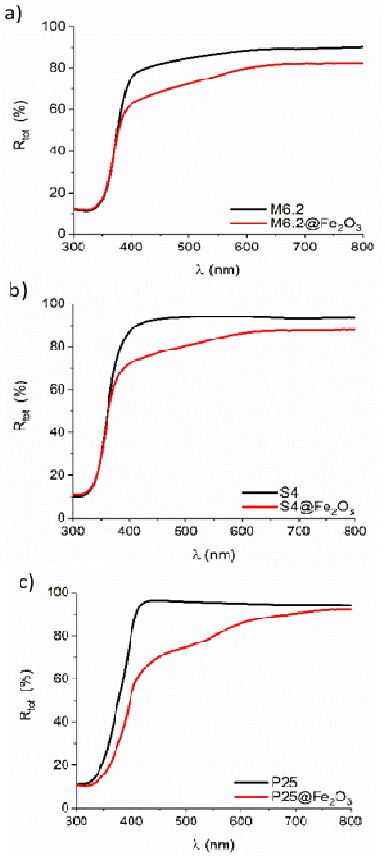

Fig. 5. Spectral dependence of total reflectance: a) TiO_2 nanocrystals and P25, b) TiO_2@Fe_2O_3 composites

Rys. 5. Spektralna zależność całkowitego współczynnika odbicia: a) nanokryształy TiO_2 i P25, b) kompozyty TiO_2@Fe_2O_3

The significant reduction in the total reflectance coefficient in the visible range of light is clear proof of the narrow band gap Fe_2O_3 deposition on the wide band gap TiO_2. The calculated band gap energies from the first derivative $dR_{tot}/d\lambda$ plots [20] (Fig. 6) are listed in Table 3. Two optical transitions (1) 3.35÷3.48 eV and (2) 3.11÷3.13 eV correspond to the band gap energies of anatase and rutile, respectively. The energy of 2.21÷÷2.30 eV (4) can be interpreted as the direct band gap of α-Fe_2O_3 [21]. The additional band gap (3) in the range of 2.85÷2.95 eV can be assigned to the acceptor level in the forbidden band of titanium(IV) oxide formed by the incorporated Fe^{3+} ions into the TiO_2 lattice [22]. What should be emphasized is that in contrast to the structural studies (XRD), the analysis of the optical properties of the TiO_2@Fe_2O_3 composites proves the presence of the iron(III) oxides phase.

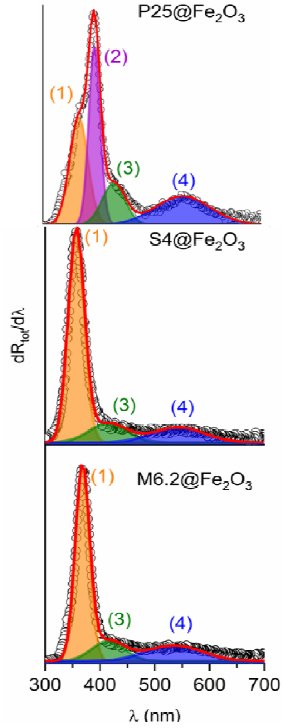

Fig. 7. Band gap energy determination from positions of maxima in first-derivative plot for TiO_2@Fe_2O_3 composites

Rys. 7. Wyznaczanie energii przerwy wzbronionej z położenia maksimów na wykresie pierwszej pochodnej dla kompozytów TiO_2@Fe_2O_3

TABLE 3. **Band-gap energy for TiO_2 and TiO_2@Fe_2O_3 composites**

TABELA 3. **Energia przerwy wzbronionej dla TiO_2 oraz kompozytów TiO_2@Fe_2O_3**

Sample	Photon energy [eV]			
	(1)	(2)	(3)	(4)
P25	3.39	3.11	-	-
P25@Fe_2O_3	3.40	3.13	2.85	2.21
S4	3.47	-	-	-
S4@Fe_2O_3	3.48	-	2.95	2.27
M6.2	3.35	-	-	-
M6.2@Fe_2O_3	3.38	-	2.94	2.30

CONCLUSIONS

The titanium(IV) oxide nanocrystals in the anatase polymorph were obtained by hydrothermal synthesis. The shape control was based on changing the TBAH-to-DEA ratio, while the number of TTIP moles remained constant. The influence of the synthesis temperature on the obtained form of nanocrystals was also investigated. At the TBAH:DEA molar ratio equal to 2:5 and synthesis temperature of 200°C, nanospheres (M1.2) composed of smaller TiO_2 crystallites were obtained. At the molar ratio of 10:1, regardless of the temperature, nanorods were obtained (M3.2, M4.2). The application of other molar ratios led to significant particle agglomeration and did not result in a distinct shape of TiO_2. The M6.2 nanocrystals prepared using an approximately 40-fold diluted shape-controlling agent and 15-fold diluted TBAH were characterized by the most uniform morphology forming nanorods with clearly distinguishable crystal facets.

In the second method, carbonate ions were responsible for shape control, and the weight fraction of KTNWs in relation to urea was increased. The microstructural studies showed that only with a small addition of the precursor (S1, S2), the amount of carbonate ions was sufficient to effectively control the shape of TiO_2. In terms of crystal structure, the anatase polymorph was obtained by the M6.2 sample, while the S4 nanocrystals were found to be a mixture of anatase with a small amount of rutile (0.3 wt.%). The band gap of the studied titanium(IV) oxide materials varied in the range of 3.35÷3.48 eV. The values of band gap energy were affected by the different sizes of the crystallites forming the nanocrystals.

The modification of TiO_2 by covering the surface with iron(III) oxide allowed a reduction in the total reflectance of the M6.2@Fe_2O_3 and S4@Fe_2O_3 composites by over 10% in the visible range of light. However, the TiO_2 nanocrystals covered with Fe_2O_3 did not show such large changes in the optical properties as in the case of the P25@Fe_2O_3 composite. This effect is related to the different proportions of high-energy surfaces in both forms of TiO_2. It was also found that the composites possess two additional optical transitions, first in the range of 2.21÷2.30 eV (Fe_2O_3 nanoparticles) and second in the range of 2.85÷2.95 eV assigned to the result of incorporating Fe^{3+} ions into the TiO_2 lattice.

Acknowledgements

M.S. has been partly supported by the EU Project POWR.03.02.00-00-I004/16.

REFERENCES

[1] Schneider J., Matsuoka M., Takeuchi M., Zhang J., Horiuchi Y., Anpo M., Bahnemann D.W., Understanding TiO_2 photocatalysis: Mechanisms and materials, Chem. Rev. 2014, 114, 9919-9986.

[2] Zhao X., Jin W., Cai J., Ye J., Li Z., Ma Y., Xie J., Qi L., Shape- and size-controlled synthesis of uniform anatase TiO_2 nanocuboids enclosed by active {100} and {001} facets, Adv. Funct. Mater. 2011, 21, 3554-3563.

[3] Ye L., Liu J., Tian L., Peng T., Zan L., The replacement of {101} by {010} facets inhibits the photocatalytic activity of anatase TiO_2, Appl. Catal. B Environ. 2013, 134-135, 60-65.

[4] Kontos A.I., Kontos A.G., Tsoukleris D.S., Bernard M.C., Spyrellis N., Falaras P., Nanostructured TiO_2 films for DSSCS prepared by combining doctor-blade and sol-gel techniques, J. Mater. Process. Technol. 2008, 196, 243-248.

[5] Euvananont C., Junin C., Inpor K., Limthongkul P., Thanachayanont C., TiO_2 optical coating layers for self-cleaning applications, Ceram. Int. 2008, 34, 1067-1071.

[6] Lin S., Li D., Wu J., Li X., Akbar S.A., A selective room temperature formaldehyde gas sensor using TiO_2 nanotube arrays, Sensors Actuators, B Chem. 2011, 156, 505-509.

[7] Menzel R., Duerrbeck A., Liberti E., Yau H.C., McComb D., Shaffer M.S.P., Determining the morphology and photocatalytic activity of two-dimensional anatase nanoplatelets using reagent stoichiometry, Chem. Mater. 2013, 25, 2137-2145.

[8] Li C., Koenigsmann C., Ding W., Rudshteyn B., Yang K.R., Regan K.P., Konezny S.J., Batista V.S., Brudvig G.W., Schmuttenmaer C.A. et al., Facet-dependent photoelectrochemical performance of TiO_2 nanostructures: An experimental and computational study, J. Am. Chem. Soc. 2015, 137, 1520-1529.

[9] Roy N., Park Y., Sohn Y., Leung K.T., Pradhan D., Green synthesis of anatase TiO_2 nanocrystals with diverse shapes and their exposed facets-dependent photoredox activity, ACS Appl. Mater. Interfaces 2014, 6, 16498-16507.

[10] Li J., Yu Y., Chen Q., Li J., Xu D., Controllable synthesis of TiO_2 single crystals with tunable shapes using ammonium--exchanged titanate nanowires as precursors, Cryst. Growth Des. 2010, 10, 2111-2115.

[11] Chen C., Hu R., Mai K., Ren Z., Wang H., Qian G., Wang Z., Shape evolution of highly crystalline anatase TiO_2 nanobipyramids, Cryst. Growth Des. 2011, 11, 5221-5226.

[12] Wu L., Yang B.X., Yang X.H., Chen Z.G., Li Z., Zhao H.J., Gong X.Q., Yang H.G., On the synergistic effect of hydrohalic acids in the shape-controlled synthesis of anatase TiO_2 single crystals, Cryst. Eng. Comm. 2013, 15, 3252--3255.

[13] Kusior A., Synowiec M., Zakrzewska K., Radecka M., Surface-controlled photocatalysis and chemical sensing of TiO_2, α-Fe_2O_3, and Cu_2O nanocrystals, Crystals 2019, 9.

[14] Mishra M., Chun D.M., α-Fe_2O_3 as a photocatalytic material: A review, Appl. Catal. A Gen. 2015, 498, 126-141.

[15] Zhang J., Kuang M., Wang J., Liu R., Xie S., Ji Z., Fabrication of carbon quantum dots/TiO_2/Fe_2O_3 composites and enhancement of photocatalytic activity under visible light, Chem. Phys. Lett. 2019, 730, 391-398.

[16] Mei Q., Zhang F., Wang N., Yang Y., Wu R., Wang W., TiO_2/Fe_2O_3 heterostructures with enhanced photocatalytic reduction of Cr(VI) under visible light irradiation. RSC Adv. 2019, 9, 22764-22771.

[17] Yang X., Liu R., Du C., Dai P., Zheng Z., Wang D., Improving hematite-based photoelectrochemical water splitting with ultrathin TiO_2 by atomic layer deposition, ACS Appl. Mater. Interfaces 2014, 6, 12005-12011.

[18] Li X., Bassi P.S., Boix P.P., Fang Y., Wong L.H., Revealing the role of TiO_2 surface treatment of hematite nanorods photoanodes for solar water splitting, ACS Appl. Mater. Interfaces 2015, 7, 16960-16966.

[19] Mansour H., Letifi H., Bargougui R., De Almeida-Didry S., Negulescu B., Autret-Lambert C., Gadri A., Ammar S., Structural, optical, magnetic and electrical properties of hematite (α-Fe_2O_3) nanoparticles synthesized by two methods: polyol and precipitation, Appl. Phys. A Mater. Sci. Process. 2017, 123, 10 pages.

[20] Kusior A., Zych L., Zakrzewska K., Radecka M., Photocatalytic activity of TiO_2/SnO_2 nanostructures with controlled dimensionality/complexity, Appl. Surf. Sci. 2019, 471, 973-985.

[21] Chernyshova I.V., Ponnurangam S., Somasundaran P., On the origin of an unusual dependence of (bio)chemical reactivity of ferric hydroxides on nanoparticle size, Phys. Chem. Chem. Phys. 2010, 12, 14045-14056.

[22] Santos R.D.S., Faria G.A., Giles C., Leite C.A.P., Barbosa H.D.S., Arruda M.A.Z., Longo C., Iron insertion and hematite segregation on Fe-doped TiO_2 nanoparticles obtained from sol-gel and hydrothermal methods, ACS Appl. Mater. Interfaces 2012, 4, 5555-5561.

